Key Points:
- A new sequence of events is found to be the result of hydraulic fracturing
- Sequence is related to multiple horizontal wells instead of just one
- Most prolific and largest magnitude fracking events to date

Correspondence to:
R. Schultz,
Ryan.Schultz@aer.ca

Hydraulic fracturing and the Crooked Lake Sequences: Insights gleaned from regional seismic networks

Ryan Schultz[1], Virginia Stern[1], Mark Novakovic[2], Gail Atkinson[2], and Yu Jeffrey Gu[3]

[1]Alberta Geological Survey, Edmonton, Alberta, Canada, [2]Department of Earth Sciences, Western University, London, Ontario, Canada, [3]Department of Physics, University of Alberta, Edmonton, Alberta, Canada

Abstract Within central Alberta, Canada, a new sequence of earthquakes has been recognized as of 1 December 2013 in a region of previous seismic quiescence near Crooked Lake, ~30 km west of the town of Fox Creek. We utilize a cross-correlation detection algorithm to detect more than 160 events to the end of 2014, which is temporally distinguished into five subsequences. This observation is corroborated by the uniqueness of waveforms clustered by subsequence. The Crooked Lake Sequences have come under scrutiny due to its strong temporal correlation (>99.99%) to the timing of hydraulic fracturing operations in the Duvernay Formation. We assert that individual subsequences are related to fracturing stimulation and, despite adverse initial station geometry, double-difference techniques allow us to spatially relate each cluster back to a unique horizontal well. Overall, we find that seismicity in the Crooked Lake Sequences is consistent with first-order observations of hydraulic fracturing induced seismicity.

1. Introduction

Earthquakes result from the rapid release of strain accumulated in the crust over geological timescales. However, it has also been understood for decades that this process can be accelerated by anthropogenic means and, for example, was suspected as the cause of earthquakes at the Rocky Mountain Arsenal [*Healy et al.*, 1968]. This suspicion was confirmed by demonstrating earthquake generation could be controlled by the injection of fluid into a well near Rangely, Colorado [*Raleigh et al.*, 1976]. To date, induced seismicity has been related to various anthropogenic applications such as dam impoundment, wastewater disposal, fluid extraction, overburden removal, enhanced geothermal systems, and hydraulic fracturing [e.g., *Davies et al.*, 2013]. Recently, focus has shifted toward understanding induced seismicity in light of the growing concern over its potential for hazard [*Ellsworth*, 2013; *Keranen et al.*, 2014; *Atkinson et al.*, 2015].

In terms of the Western Canada Sedimentary Basin (WCSB), natural seismicity is sparse and quiescent [e.g., *Stern et al.*, 2013; *Schultz et al.*, 2015]. The WCSB has an interesting history of seismically active clusters recognized near the town of Rocky Mountain House [*Rebollar et al.*, 1982, 1984; *Wetmiller*, 1986], the Brazeau River [*Schultz et al.*, 2014], Fort St. John [*Horner et al.*, 1994], Turner Valley, Kinbasket Lake [*Ellis and Chandra*, 1981], the Horn River Basin [*BC Oil and Gas Commission*, 2012, 2014; *Farahbod et al.*, 2015], and Cardston. Many of these aforementioned clusters have been conjectured as induced by gas extraction [*Baranova et al.*, 1999], wastewater disposal [*Milne*, 1970; *Horner et al.*, 1994; *Schultz et al.*, 2014], or hydraulic fracturing operations [*BC Oil and Gas Commission*, 2012, 2014; *Farahbod et al.*, 2015]. In the winter of 2013 operators hydraulically fractured a well on 26 November, just west of Crooked Lake, which is ~30 km west of the town of Fox Creek, Alberta, Canada. During operations at this well, a new sequence of earthquakes was recorded on regional seismic networks beginning 1 December 1:38:08 UTC. To date, these sequences of events are among the most prolific and highest magnitude earthquakes suspected as induced by hydraulic fracturing (HF). In this paper, we assert that these recent earthquakes are the result of nearby HF operations. To make this claim, temporal patterns in seismicity are analyzed and correlated to the timing of nearby HF treatment stages. We find that the timing of events is coordinated in subsequences, which are highly related to nearby HF operations at multiple wells. Furthermore, full waveform correlation methods are able to characterize the subsequences and thus differentiate between them. Despite distant station geometry (100+ km), robust double-difference epicenters are able to reasonably delineate trends in earthquake geometry and connect subsequence events with their corresponding well. This is accomplished by using continuous waveform data amalgamated from various
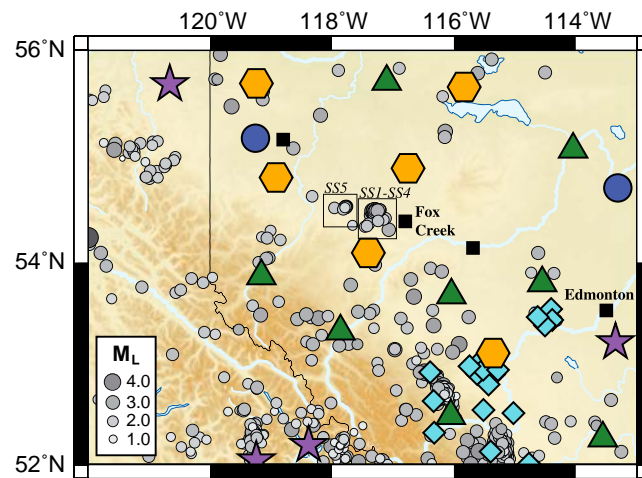
Figure 1. Map depicting locations of seismic stations relevant to this study, separated by network: RAVEN (orange hexagons), CRANE (green triangles), TD (cyan diamonds), CNSN (purple stars), and ATSN (blue circles). Note that RAVEN stations were installed during the summer of 2014, and thus, the data were only available for later subsequences (SS5). Locations of cities (black squares) are superimposed for geographic reference alongside regionally catalogued [*Earthquakes Canada*, 2012; *Stern et al.*, 2013] seismicity (gray circles). The earthquake sequences focused on in this paper have been highlighted by boxes in this figure.

regional networks (Figure 1) including the Canadian National Seismic Network (CNSN), the Canadian Rockies and Alberta Network (CRANE) [*Gu et al.*, 2011], Regional Alberta Seismic Observatory for Earthquake Studies Network (RAVEN), the TransAlta Dam Network (TD), and the Alberta Telemetered Seismic Network (ATSN) [*Eaton*, 2014]. Finally, we compare and contrast this sequence of events to other case studies and not only find similarities in the timing and magnitude of events but also note a difference: events in our study region appear to be induced from multiple, different wells, and these differences can be observed seismically. Overall, we conclude that the most likely cause of these events is their induction from adjacent HF operations.

2. Seismicity Patterns and Hydraulic Fracturing Operations

Within central Alberta, the Duvernay Formation is a Frasnian-aged, organic-rich shale which has recently been exploited by unconventional drilling and completion technologies. This paper focuses on horizontal, multistage wells in the Waskahigan and McKinley fields, ~30 km west of the town of Fox Creek, Alberta, which underwent hydraulic fracturing of the Duvernay. In the study region, the Duvernay is logged at an average ~3400 m depth, and 40 m thickness. To access the hydrocarbons within the Duvernay, hydraulic fracturing operations consists of multistaged pressure treatments of acid-spotted perforations. For example, average HF treatment stages in the region have mean pressures, pumping rates, total pumped fluid volume, and proppant weight in well of 60 MPa, 9 m^3/min, 2700 m^3, and 200 tonnes, respectively.

Despite more than 3000 HF well completions in Alberta during 2013, three horizontal wells are the focus of this study. These wells are exceptional as they occur simultaneous to nearby clustered earthquakes (Figure 2a) known as the Crooked Lake Sequences (CLS). Events from the CLS range in magnitude from 1.7–3.9 M_W, determined via pseudoacceleration amplitudes and a stochastic point source-based scaling relationship [*Atkinson and Mahani*, 2013; *Atkinson et al.*, 2014]. Due to the regional aperture of recording stations in the Crooked Lake region, the detection threshold of catalogued events restricts our ability to confidently discern temporal patterns in seismicity. To address this issue, we utilize a matched filter algorithm [*Schaff*, 2008] with five template earthquakes to extend the detection threshold of events in the CLS [*Schaff and Waldhauser*, 2010]. Our search window begins 1 November 2013, ~1 month before the first recorded event in the CLS and ends 31 December 2014. Although the scope of this study is restricted to the end of 2014 calendar year, the CLS continues to be seismically active with a 3.9 M_W event (4.4 M_L) recorded as the largest to date (23 January 2014 6:49:18 UTC); the magnitude of the M_W 3.9 is obtained from both the pseudoacceleration amplitude technique [*Atkinson et al.*, 2014] and from a regional moment tensor (W. Greig, Nanometrics, personal communication, 2015). From the extended CLS catalogue, we note that seismicity is punctuated into five temporally distinct subsequences (abbreviated SS1–SS5) of increased seismic activity (Figure 2a). Coincidently, hydraulic fracturing stimulations occur simultaneous to these subsequences and the corresponding Crooked Lake wells are abbreviated accordingly (CLW1–CLW3). For example, the first located event in SS1 is 1 December 2013 1:38:08 UTC, during stage 8/20 in CLW1 (Figure 2b). After the initiation of SS1, events were recorded frequently until HF operations at the CLW1 were temporarily suspended after 4 December. Similar observations are made in February for SS2/CLW2 and May for SS3/CLW3 (Figure 2c). Interestingly, SS4 occurs as the operations at CLW1 are resumed in May and is thus an exception to our adopted naming convention. It is important to note to the reader that while the August events of SS5 probably have a
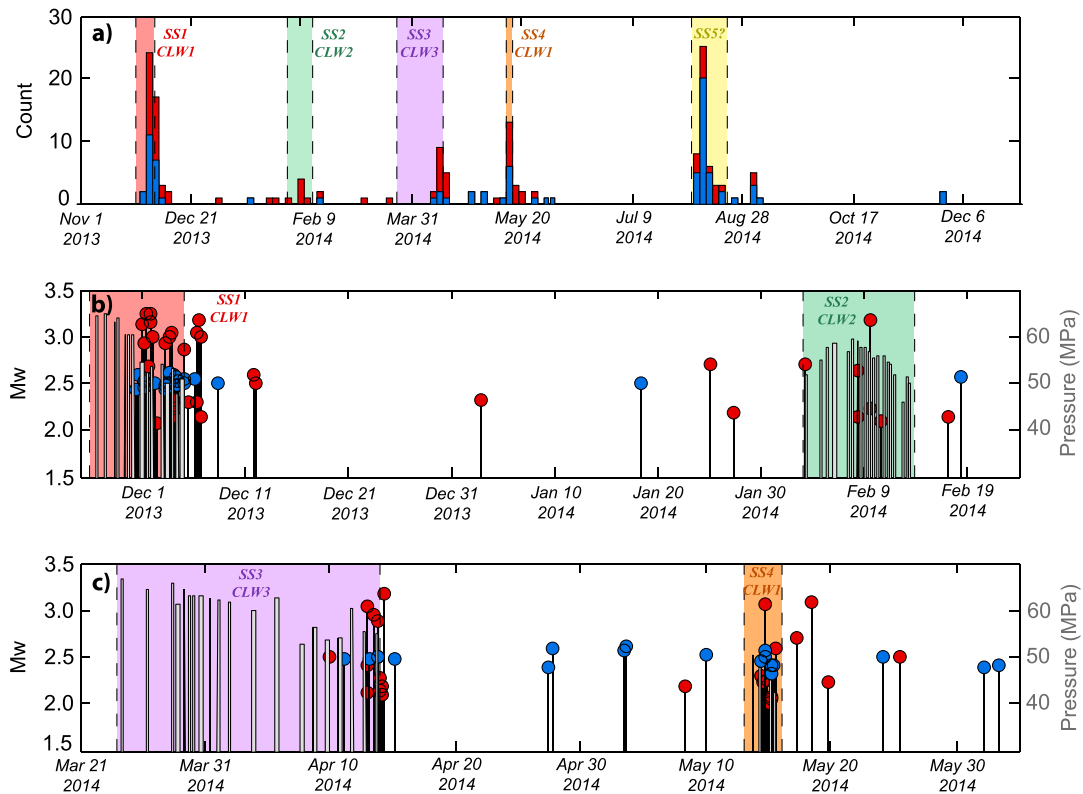
Figure 2. Timing of CLS earthquakes and hydraulic fracturing completions. (a) Histogram of located seismicity (red bars) and extended catalogue from cross correlation (blue bars). HF schedules are bounded by colored boxes and labeled with respective subsequence and well. (b) Moment magnitudes of located (red circles) and detected (blue circles) earthquakes are compared to average injection pressure during HF stages (gray bars). (c) Plot similar to previous for later well completions, all panels use the same color convention for HF schedule boxes.

corresponding well like SS1–SS4, this study is unable to investigate due to 1+ year period of well data confidentiality. Lastly, we place a statistical confidence on the relationship between seismic activity and hydraulic fracturing operations by cross-correlation reshuffling tests [*Telesca*, 2010]. We find that the best correlation for the timing of all subsequences and suspected fracturing stimulations in the CLS has a confidence greater than 99.99%.

3. Multiplicity of the CLS

It is well recognized that station geometry affects the resolution of hypocenter location. In the case of the CLS, the majority of stations involved in earthquake location are at regional distances (100+ km, see Figure 1). To glean as much information as possible about the CLS, we examine the waveform signature of recorded events using the Gephysical Institute Seismology MATLAB Objects suite [*Reyes and West*, 2011]. Traces are band-pass filtered at corners of 0.8–5.0 Hz, and we compare, chronologically, the full waveform cross-correlations of all possible event pairings.

The correlation of more than 75 earthquake waveforms reveals trends consistent with the temporally inferred subsequences (Figure 2). The multiplicity of events in the CLS distinguishes itself into the same five subsequences. Furthermore, the timing of these multiplets is coincident with HF operations and the intrasubsequence events are observed to be highly correlated, repeated earthquakes (Figure 3a). For example, the averaged correlation coefficient (CC) within subsequences is 0.94, 0.81, 0.88, 0.86, and 0.84 for SS1–SS5, respectively. On the other hand, intersubsequence pairings are found to have almost no consistency (<0.30 CC), with the exception of events from SS1 and SS4 that show a smaller degree of similarity (0.63 averaged CC). Interestingly, events outside of the subsequence windows show sporadic similarity to their prior HF multiplet. This feature of the CLS is most clearly demonstrated in the waveform multiplicity of SS1 during stimulation and after shut-in (Figure 3b): there is a high degree of multiplicity during the December HF stages of CLW1; once stimulation is
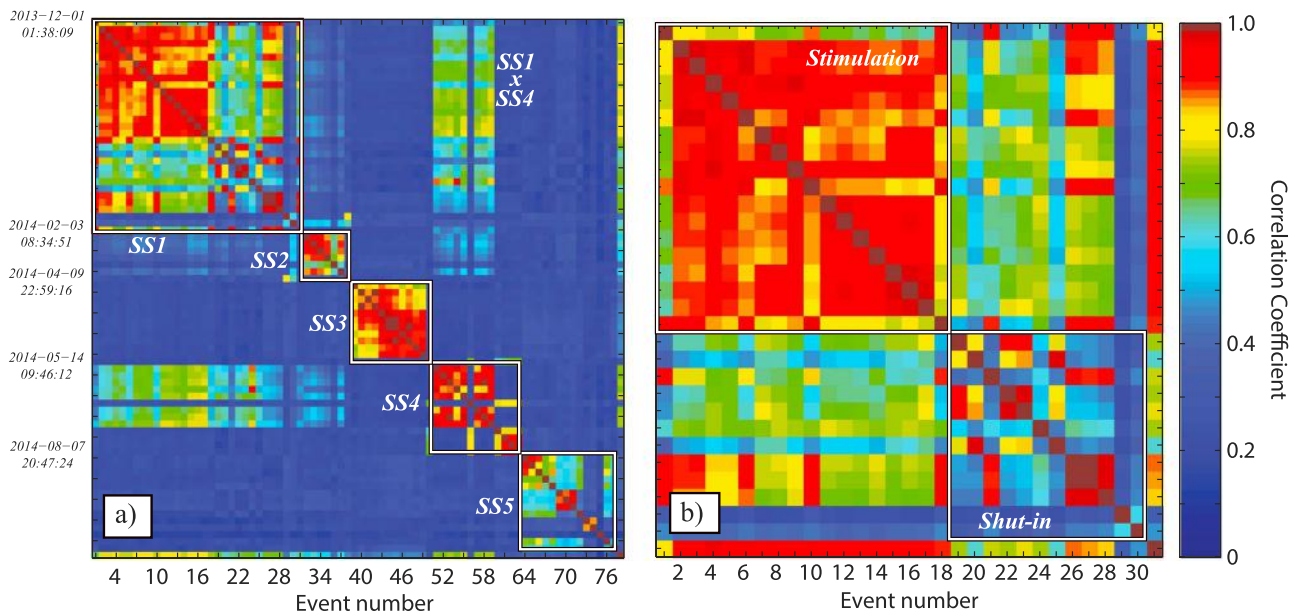
Figure 3. (a) Cross correlations of all possible event pairs in the CLS ordered chronologically, diagonal matrix elements represent waveform autocorrelations. For clarity, event correlations have been segregated according to their respective subsequences (white boxes), with origin times of first located subsequence event labeled on the y axis. (b) The second panel further dissects SS1: events are segregated into highly correlated events during CLW1 stimulation, and sporadically correlated events during CLW1 shut-in. In both panels the final matrix element is the beam average; thus, the last row/column are the CLS or SS1 beam paired with individual events.

discontinued the post-HF events spuriously resemble stimulation events. However, it is worth noting that while shut-in events do not resemble each stimulation event individually; they do resemble (0.71 averaged CC) the beam average of stimulation events (Figure 3b).

4. Robust Earthquake Relocations

To further investigate the nature of the CLS, we utilize the program HypoDD [*Waldhauser and Ellsworth*, 2000; *Waldhauser*, 2001] to discern the distribution of epicentral locations. Input locations are based on relocation [*Pavlis et al.*, 2004] of CLS events with a local velocity model and an assumed hypocentral depth of 3 km (see Figure 1). The local velocity model is a composition of nearby well log data and CRUST1.0 [*Laske et al.*, 2013]. Overall, the phase arrival pairings of 64 events from SS1 to SS4 results in more than 8400 P and 2400 S catalogue differential times as well as 8400 P and 1300 S waveform differential lags. Inversion of SS5 is handled separately from the remaining subsequences due to a clear westward bias in event locations, poor correlation to other subsequences, and increased station density. To account for relative instability of results, we apply a bootstrap methodology [*Efron and Tibshirani*, 1986]: A subset of 80% of the input earthquakes are selected randomly for a trial inversion and this trial inversion is then repeated 1000 times. Individual hypocenter parameters are obtained from the statistical distribution of trial locations, with robust locations and their error from the modal values and standard deviation, respectively. Hypocenter locations which are multimodal, have exceptional error, or are unstable are discarded.

After obtaining robust, stable results we retain 60 events from the CLS (Table 1). The double-difference relocations of SS1–SS4 are clustered 5 km NW of Crooked Lake and trends in the epicentral relocations mimic the geometry of the wells in this study (Figure 4). In particular, events from SS1 to SS2 are predominantly centered on CLW1 and CLW2 and are located within ~1.5 and 3.0 km of their respective well trajectories. As well, events from SS4 form a linear feature from the heel of the CLW1 to ~6 km NE. Of the considered subsequences, SS3 has the greatest lateral bias in event relocations: events are centered ~5 km NE of the CLW3. Due to only a couple of robust observations for SS3, we are unable to confidently comment if this bias is a systematic trend, or simply an artifact of too few data. While stimulation-related events generally tend to their suspected wells, shut-in events tend to have more spurious relocations throughout the CLS region. Likely this is due to larger location uncertainty due to poorer event pair correlations associated with shut-in events. The last

Table 1. Robust Double-Difference Earthquake Locations

Date (yyyy/mm/dd)	Time (UTC) (hh:mm:ss.ss)	Latitude (°)	Longitude (°)	Depth (km)	M_W
2013/12/01	01:38:05.02	54.503012 ± 0.005636	−117.300050 ± 0.049912	2.2 ± 1.0	3.13
2013/12/01	05:26:29.72	54.497539 ± 0.006197	−117.302451 ± 0.046025	1.8 ± 1.4	2.92
2013/12/01	10:06:22.70	54.496608 ± 0.005832	−117.305736 ± 0.053887	4.5 ± 1.2	3.25
2013/12/01	15:09:24.69	54.495438 ± 0.006099	−117.300128 ± 0.046466	1.9 ± 1.3	2.67
2013/12/01	19:12:38.60	54.497531 ± 0.005725	−117.287079 ± 0.070141	1.2 ± 1.8	2.51
2013/12/01	20:26:21.54	54.476592 ± 0.010862	−117.232042 ± 0.109982	5.2 ± 1.1	3.16
2013/12/02	02:51:50.73	54.492037 ± 0.006161	−117.296811 ± 0.045141	2.5 ± 1.5	3.00
2013/12/02	08:41:38.56	54.487707 ± 0.006170	−117.308722 ± 0.051502	4.2 ± 1.3	2.07
2013/12/03	06:27:52.08	54.497823 ± 0.006223	−117.294662 ± 0.049205	1.9 ± 1.4	2.93
2013/12/03	12:59:32.64	54.490537 ± 0.006125	−117.306776 ± 0.045141	3.2 ± 1.3	2.50
2013/12/03	16:04:08.74	54.472821 ± 0.006517	−117.336330 ± 0.044788	5.2 ± 1.3	3.00
2013/12/03	18:45:06.36	54.491362 ± 0.006152	−117.303657 ± 0.052739	1.8 ± 1.5	2.14
2013/12/03	21:37:19.28	54.454183 ± 0.006651	−117.355280 ± 0.043640	4.1 ± 1.1	3.03
2013/12/04	00:48:43.92	54.486190 ± 0.006303	−117.315187 ± 0.048498	2.9 ± 1.2	2.60
2013/12/04	03:13:16.44	54.493215 ± 0.006579	−117.305810 ± 0.047880	1.6 ± 1.9	2.33
2013/12/04	09:58:23.10	54.496333 ± 0.005716	−117.305519 ± 0.054594	1.6 ± 1.6	2.50
2013/12/05	00:02:05.09	54.486948 ± 0.006214	−117.297625 ± 0.061661	2.3 ± 1.4	2.85
2013/12/05	13:46:08.51	54.486034 ± 0.006232	−117.329124 ± 0.048410	4.7 ± 1.3	2.30
2013/12/06	06:14:00.45	54.503093 ± 0.006143	−117.297973 ± 0.052915	3.4 ± 1.2	3.10
2013/12/06	06:35:19.47	54.483859 ± 0.006481	−117.343632 ± 0.054859	5.1 ± 1.3	3.04
2013/12/06	14:22:12.16	54.492335 ± 0.006072	−117.315269 ± 0.048675	2.8 ± 1.0	3.18
2013/12/06	15:51:15.75	54.492034 ± 0.006339	−117.290627 ± 0.053269	1.7 ± 1.5	2.99
2013/12/06	17:57:52.12	54.497061 ± 0.005556	−117.284239 ± 0.059187	1.4 ± 0.8	2.13
2013/12/11	21:40:26.96	54.496555 ± 0.006223	−117.340901 ± 0.049293	4.6 ± 1.1	2.60
2013/12/12	01:59:37.20	54.497226 ± 0.006197	−117.323001 ± 0.050530	2.3 ± 1.3	2.50
2014/01/02	20:34:34.72	54.498709 ± 0.006330	−117.321418 ± 0.047968	4.8 ± 1.0	2.31
2014/01/25	03:59:40.88	54.483483 ± 0.006090	−117.252995 ± 0.055212	4.2 ± 0.8	2.70
2014/01/27	09:37:55.36	54.456184 ± 0.006455	−117.315300 ± 0.046201	5.6 ± 1.1	2.19
2014/02/03	08:34:47.52	54.501228 ± 0.006001	−117.299285 ± 0.049470	2.3 ± 1.2	2.70
2014/02/08	08:56:29.38	54.459744 ± 0.006027	−117.280849 ± 0.056272	7.2 ± 1.2	2.15
2014/02/08	11:23:19.20	54.471347 ± 0.005716	−117.245097 ± 0.060601	3.9 ± 0.9	2.63
2014/02/09	14:00:41.46	54.454681 ± 0.006152	−117.323821 ± 0.053622	9.4 ± 0.8	2.23
2014/02/09	14:23:39.31	54.478485 ± 0.006473	−117.298301 ± 0.056979	5.1 ± 1.1	3.18
2014/02/17	01:51:29.85	54.466951 ± 0.006250	−117.319668 ± 0.048410	4.9 ± 1.2	2.15
2014/03/10	09:34:53.38	54.463404 ± 0.006464	−117.317610 ± 0.047438	4.5 ± 1.2	2.14
2014/04/14	02:19:47.26	54.422191 ± 0.006820	−117.124342 ± 0.093463	3.6 ± 0.6	2.09
2014/04/14	03:23:44.29	54.411544 ± 0.006749	−117.150528 ± 0.084982	3.6 ± 0.7	2.18
2014/05/14	09:46:07.81	54.497351 ± 0.006099	−117.273589 ± 0.046643	2.9 ± 1.3	2.29
2014/05/14	15:30:21.41	54.508282 ± 0.006099	−117.204270 ± 0.047350	1.5 ± 1.7	2.23
2014/05/14	19:26:56.08	54.499911 ± 0.005778	−117.235739 ± 0.046025	4.0 ± 0.9	3.06
2014/05/14	22:09:11.98	54.493204 ± 0.005992	−117.296529 ± 0.057862	3.0 ± 1.4	2.25
2014/05/15	02:13:17.55	54.509139 ± 0.005734	−117.215458 ± 0.052650	3.4 ± 0.9	2.01
2014/05/15	04:57:08.54	54.343544 ± 0.011467	−117.458116 ± 0.141343	6.5 ± 2.5	2.06
2014/05/15	06:45:28.75	54.498322 ± 0.005725	−117.300054 ± 0.043375	3.7 ± 1.0	2.08
2014/05/15	11:58:16.90	54.497410 ± 0.006205	−117.249246 ± 0.053799	4.6 ± 1.1	2.60
2014/05/17	07:47:05.06	54.371243 ± 0.007114	−117.398170 ± 0.113428	7.7 ± 1.7	2.70
2014/05/18	11:48:24.01	54.397785 ± 0.009562	−117.243190 ± 0.223675	7.6 ± 2.6	3.08
2014/05/19	20:26:23.98	54.351582 ± 0.007354	−117.426603 ± 0.156537	10.3 ± 1.6	2.22
2014/08/07	20:47:24.92	54.541610 ± 0.001603	−117.754924 ± 0.021908	3.0 ± 0.6	2.10
2014/08/08	07:37:40.54	54.536499 ± 0.001487	−117.776481 ± 0.021731	2.2 ± 0.5	2.35
2014/08/08	18:08:42.88	54.533521 ± 0.002324	−117.763281 ± 0.035247	4.9 ± 0.6	1.95
2014/08/09	07:40:08.73	54.531335 ± 0.002475	−117.774064 ± 0.027739	4.4 ± 0.6	3.83
2014/08/09	08:07:53.07	54.540987 ± 0.001611	−117.782104 ± 0.022350	1.8 ± 0.5	2.10
2014/08/09	22:18:36.48	54.532646 ± 0.001781	−117.784847 ± 0.022880	3.0 ± 0.8	2.40
2014/08/10	08:06:21.66	54.533997 ± 0.001763	−117.778247 ± 0.022527	4.1 ± 0.8	2.30
2014/08/10	12:33:25.58	54.531364 ± 0.002386	−117.780884 ± 0.024823	4.4 ± 0.6	2.21
2014/08/13	10:47:46.24	54.534603 ± 0.002475	−117.771419 ± 0.027650	4.1 ± 0.7	2.20
2014/08/18	05:02:32.35	54.357052 ± 0.002787	−117.661621 ± 0.083922	3.5 ± 1.4	2.20
2014/08/31	21:39:54.60	54.508655 ± 0.002146	−117.814168 ± 0.023763	4.5 ± 0.5	2.72
2014/09/02	16:48:52.96	54.524418 ± 0.002074	−117.790609 ± 0.023145	3.2 ± 0.9	2.34
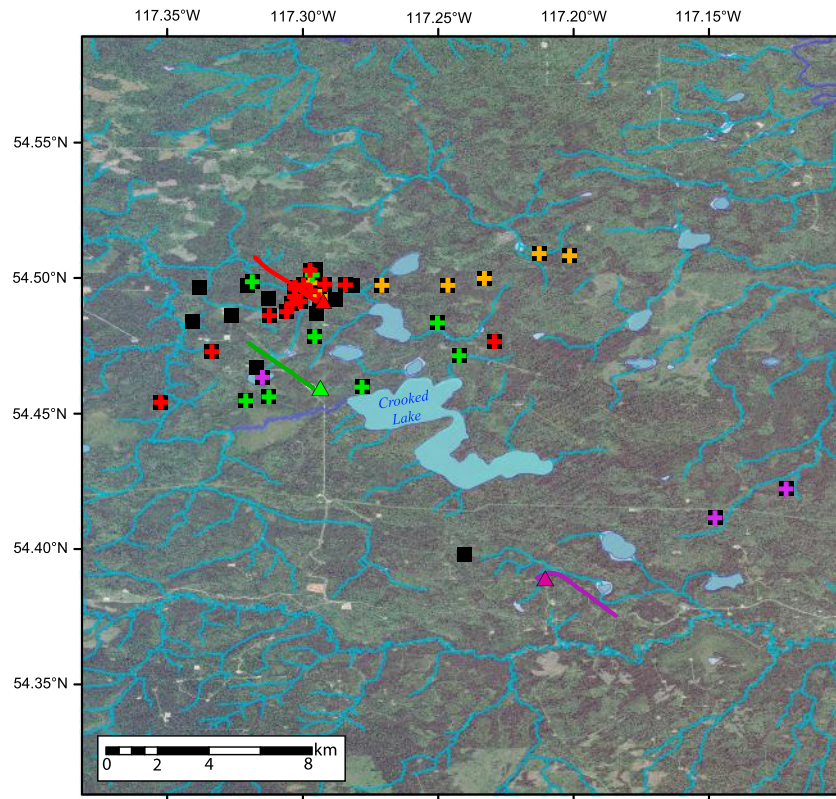
Figure 4. Spatial distribution of robust, double-difference epicenters (black squares) in relation to Crooked Lake, before RAVEN was available. To highlight trends in locations, epicenters have been binned according to timing of well stimulation for SS1 (red crosses), SS2 (green crosses), SS3 (purple crosses), and SS4 (orange crosses). Events without crosses occurred during shut-in periods. Surface locations of relevant wells are labeled by triangles, with lines depicting horizontal well trajectory. Wells are color coordinated with their respective subsequences, i.e., CLW1 is red, CLW2 is green, and CLW3 is purple.

of our considered subsequences, SS5, is located ~65 km WNW of Fox Creek and benefits from additional constraints from recently installed RAVEN stations (Figure 5). Events in SS5 are tightly clustered around a point and vary within (1 standard epicentral error) 600 m of the centroid. Despite less than optimal station distance, rudimentary constraints on depth places the average at 3.4 ± 1.1 km, within the basal Paleozoic sedimentary units at a depth similar to the regional Duvernay Formation depth. A similar general trend in source depths is also observed for previous subsequences (SS1–SS4), albeit with greater variance in their locations.
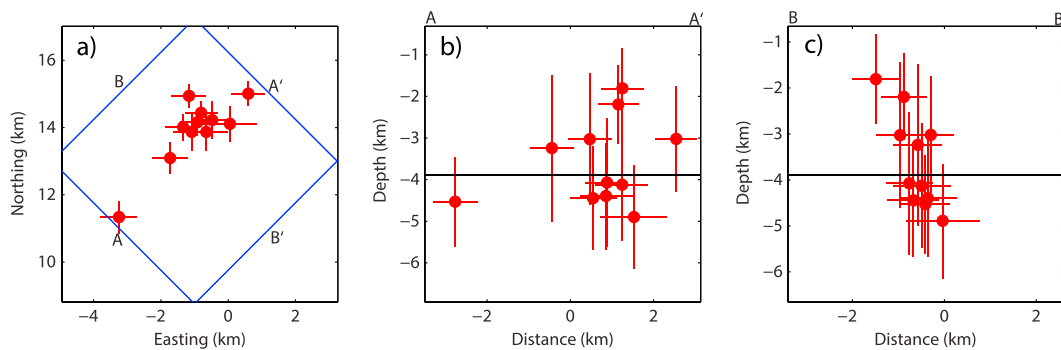
Figure 5. Double-difference relocation of SS5 events (red circles) using bootstrap statistics with standard errors depicted by crosshair length (0.95 confidence interval). (a) Aerial view of epicenter locations. (b) Depth cross-section A to A' trending from SW to NE. (c) Cross-section trending from NE to SW showing the depth distribution of relocated hypocenters. Horizontal black line in Figures 5b and 5c denotes the depth at the top of the Precambrian basement. Depth profiles are oriented according to the regional stress field, where A-A' is parallel with the maximum horizontal stress [*Reiter et al.*, 2014].

5. Discussions

Observation of a direct correlation between HF stimulation and seismic response supports the argument of a causal link between these two processes [e.g., *Davis and Frohlich*, 1993; *Oprsal and Eisner*, 2014]. In fact, our statistical reshuffling tests place a confidence greater than 99.99% of a time-delayed correlation between HF operations (CLW1–CLW3) and respondent seismicity (SS1–SS4). While this confidence interval is a statistically strong correlation, additional considerations strengthen the plausibility of a causal link. For example, the CLW3 stimulation report describes a screen-out (i.e., an interruption in the flow of HF slurry that causes a shutdown of injection operations) during the twelfth stage, after which, this and proceeding stages stimulated at reduced injection rates (~8 m^3/min, stages 12–17), and stimulations resumed at nominal injection rates for remaining stages (~11 m^3/min, stages 18–20). A possible conjecture for the observation of a screen-out at CLW3 is the unwanted flow of HF fluid into a preexisting fault system. Coincidentally, the first event in SS3 follows the sixteenth stage, with a greater rate of earthquakes detected after the nineteenth stage; this rate diminishes drastically ~12 h after the final stage is completed. Similarly, earthquakes purported as induced by hydraulic fracturing operations in Lancashire, England, and Poland Township, Ohio, noted a similar screen-out in completion reports for stages immediately preceding observed seismicity [*Clarke et al.*, 2014; *Skoumal et al.*, 2015]. In another example, operations at CLW1 were suspended prematurely, shortly after the first SS1 earthquakes (~5 days), with reports indicating completion of only the initial 15/20 stages. These remaining five stages were completed months later, contemporaneously with SS4. Interestingly, waveform similarity of SS1 and SS4 is evidenced (see Figure 3a) suggesting these two subsequences' hypocenters are nearby and have similar fault motions. This similarity is consistent with an induction process driven by CLW1 stimulations: nucleation of fault slip repeats with escalating pore pressure, when stimulation ceases pore pressure-induced events cease and only continue rupturing after the prior pressures are exceeded [*Kaiser*, 1950].

The premature shut-in of CLW1 provides an opportunity to scrutinize spatial and temporal patterns of stimulation versus shut-in events for the CLS. During hydraulic fracturing, the propagation of a microseismic cloud depends on the hydraulic diffusivity of the rock matrix [*Shapiro and Dinske*, 2009]. Slip is first initiated on critically stressed faults nearby the stimulation source, and earthquakes are later triggered further from the source as the pore pressure front diffuses [e.g., *Albaric et al.*, 2014]. Continued stimulation may induce repetitions of earthquakes given sufficient pore pressure increases [e.g., *Goertz-Allmann and Wiemer*, 2013]. These phenomena are consistent with the repetition of highly similar earthquakes observed during CLW1 stimulation (see Figure 3b). However, SS1 events depart from this trend following shut-in of CLW1. Shut-in events have sporadic waveform similarity but retain the overall consistency to the SS1 beam, which suggests that these events are located about the mean hypocenter of SS1. This observation has a potential explanation via a seismic back-front [*Parotidis et al.*, 2004]: during shut-in, events are no longer observed near the stimulation source due to reduced pore pressure. Instead, events are only observed in the region between the still growing pore pressure front and the reduced pore pressure back-front.

Lastly, the close lateral proximity of CLS subsequences and horizontal well trajectories further suggests a causal mechanism. During typical hydraulic fracturing operations, significant pore pressure changes are expected up to hundreds of meters from the HF interval [e.g., *Davies et al.*, 2012, 2013]. However, the presence of a preexisting fault provides a means of hydraulic communication to distant and potentially critically stressed faults [*Barton et al.*, 1995; *Zhang et al.*, 2013]. Despite adverse station geometry, double-difference epicenters trend about their associated wells (see Figure 4). We do note that lateral biases of ~5 km are evidenced for CLW3/SS3. Similarly, lateral differentials of ~2.5 km were reported between induced seismicity and HF well in the Eola Field, Oklahoma [*Holland*, 2013]. In addition, our constraints on focal depth for events in the CLS (e.g., see Figure 5c) place events within the Paleozoic sedimentary units and upper crystalline basement. Similarly, case studies of regionally observed seismicity associated with hydraulic fracturing have reported similar trends in hypocenter depths, occurring at or below the fracturing interval [*de Pater and Baisch*, 2011; *Holland*, 2011, 2013; *Clarke et al.*, 2014; *Friberg et al.*, 2014; *Skoumal et al.*, 2015].

6. Conclusions

At least 160 earthquakes were detected in the CLS region since hydraulic fracturing operations began to January of 2015. This region previously experienced limited seismicity before the onset of events in December 2013. The timing of CLS events and hydraulic fracturing operations are highly correlated (>99.99%), suggesting

a relationship between the two. This claim is further corroborated by the investigation of waveform correlations, which shows that earthquakes from CLW1 stop when fracturing stops, and continue when fracturing resumes months later. Despite unfavorable station geometry, locations of events are reasonably well constrained and are proximal to their associated wells at distances comparable to other case studies. We conclude that CLS seismicity within our study period is most likely due to hydraulic fracturing of the Duvernay Formation. Today, the CLS is still active; likely, these new subsequences are also linked to hydraulic fracturing operations, in light of our findings.

References

Albaric, J., V. Oye, N. Langet, M. Hasting, I. Lecomte, K. Iranpour, M. Messeiller, and P. Reid (2014), Monitoring of induced seismicity during the first geothermal reservoir stimulation at Paralana, Australia, *Geothermics*, *52*, 120–131, doi:10.1016/j.geothermics.2013.10.013.

Atkinson, G. M., and A. B. Mahani (2013), Estimation of moment magnitude from ground motions at regional distances, *Bull. Seismol. Soc. Am.*, *103*(1), 107–116, doi:10.1785/0120120182.

Atkinson, G. M., D. W. Greig, and E. Yenier (2014), Estimation of moment magnitude (M) for small events (M < 4) on local networks, *Seismol. Res. Lett.*, *85*(5), 1116–1124, doi:10.1785/0220130180.

Atkinson, G. M., H. Ghofrani, and K. Assatourians (2015), Impact of induced seismicity on the evaluation of seismic hazard: Some preliminary considerations, *Seismol. Res. Lett.*, *86*(3), doi:10.1785/0220140204.

Baranova, V., A. Mustaqeem, and S. Bell (1999), A model for induced seismicity caused by hydrocarbon production in the Western Canada sedimentary basin, *Can. J. Earth Sci.*, *36*(1), 47–64, doi:10.1139/e98-080.

Barton, C. A., M. D. Zoback, and D. Moos (1995), Fluid flow along potentially active faults in crystalline rock, *Geology*, *23*(8), 683–686, doi:10.1130/0091-7613(1995)023<0683:FFAPAF>2.3.CO;2.

BC Oil and Gas Commission (2012), Investigation of observed seismicity in the Horn River Basin, p. 29. [Available at http://www.bcogc.ca/document.aspx?documentID=1270.]

BC Oil and Gas Commission (2014), Investigation of observed seismicity in the Montney trend, 32 pp. [Available at http://www.bcogc.ca/sites/default/files/documentation/technical-reports/investigation-observed-seismicity-montney-trend.pdf.]

Clarke, H., L. Eisner, P. Styles, and P. Turner (2014), Felt seismicity associated with shale gas hydraulic fracturing: The first documented example in Europe, *Geophys. Res. Lett.*, *41*, 8308–8314, doi:10.1002/2014GL062047.

Davies, R. J., S. A. Mathias, J. Moss, S. Hustoft, and L. Newport (2012), Hydraulic fractures: How far can they go?, *Mar. Pet. Geol.*, *37*(1), 1–6, doi:10.1016/j.marpetgeo.2012.04.001.

Davies, R., G. Foulger, A. Bindley, and P. Styles (2013), Induced seismicity and hydraulic fracturing for the recovery of hydrocarbons, *Mar. Pet. Geol.*, *45*, 171–185, doi:10.1016/j.marpetgeo.2013.03.016.

Davis, S. D., and C. Frohlich (1993), Did (or will) fluid injection cause earthquakes? Criteria for a rational assessment, *Seismol. Res. Lett.*, *64*, 207–224, doi:10.1785/gssrl.64.3-4.207.

de Pater, C. J., and S. Baisch (2011), Geomechanical study of Bowland Shale seismicity, Synthesis Report, p. 57.

Earthquakes Canada (2012), GSC, Earthquake Search (On-line Bulletin). [Available at http://earthquakescanada.nrcan.gc.ca/stndon/NEDB-BNDS/bull-eng.php, Nat. Res. Can., December 2012.]

Eaton, D. (2014), Alberta Telemetered Seismograph Network (ATSN): Real-time monitoring of seismicity in northern Alberta, *CSEG Rec.*, *39*(3), 30–33.

Efron, B., and R. Tibshirani (1986), Bootstrap methods for standard errors, confidence intervals, and other measures of statistical accuracy, *Stat. Sci.*, *1*(1), 54–75, doi:10.1214/ss/1177013815.

Ellis, R. M., and B. Chandra (1981), Seismicity in the Mica Reservoir (McNaughton Lake) area: 1973–1978, *Can. J. Earth Sci.*, *18*, 1708–1716, doi:10.1139/e81-157.

Ellsworth, W. L. (2013), Injection-induced earthquakes, *Science*, *341*, 6142, doi:10.1126/science.1225942.

Farahbod, A. M., H. Kao, D. M. Walker, and J. F. Cassidy (2015), Investigation of regional seismicity before and after hydraulic fracturing in the Horn River Basin, northeast British Columbia, *Can. J. Earth Sci.*, *52*(2), 112–122, doi:10.1139/cjes-2014-0162.

Friberg, P. A., G. M. Besana-Ostman, and I. Dricker (2014), Characterization of an earthquake sequence triggered by hydraulic fracturing in Harrison County, Ohio, *Seismol. Res. Lett.*, *85*(2), 462, doi:10.1785/0220140127.

Goertz-Allmann, B. P., and S. Wiemer (2013), Geomechanical modeling of induced seismicity source parameters and implications for seismic hazard assessment, *Geophysics*, *78*, KS25–KS39, doi:10.1190/geo2012-0102.1.

Gu, Y. J., A. Okeler, L. Shen, and S. Contenti (2011), The Canadian Rockies and Alberta Network (CRANE): New constraints on the Rockies and Western Canada Sedimentary Basin, *Seismol. Res. Lett.*, *82*, 575–588, doi:10.1785/gssrl.82.4.575.

Healy, J. T., W. W. Rubey, D. T. Griggs, and C. B. Raleigh (1968), The Denver earthquakes, *Science*, *161*, 1301–1310, doi:10.1126/science.161.3848.1301.

Holland, A. A. (2011), Examination of possibly induced seismicity from hydraulic fracturing in the Eola Field, Garvin County, Oklahoma, *Oklahoma Geol. Surv. Open File Rep., OF1–2011*, 31 pp.

Holland, A. A. (2013), Earthquakes triggered by hydraulic fracturing in south-central Oklahoma, *Bull. Seismol. Soc. Am.*, *103*, 1784–1792, doi:10.1785/0120120109.

Horner, R. B., J. E. Barclay, and J. M. MacRae (1994), Earthquakes and hydrocarbon production in the Fort St. John area of northeastern British Columbia, *Can. J. Explor. Geophys.*, *30*, 39–50.

Kaiser, J. (1950), Untersuchungen über das Auftreten von Geräuschen beim Zugversuch, PhD thesis, Technische Hochschule München.

Keranen, K. M., M. Weingarten, G. A. Abers, B. A. Bekins, and S. Ge (2014), Sharp increase in central Oklahoma seismicity since 2008 induced by massive wastewater injection, *Science*, *345*(6195), 448–451, doi:10.1126/science.1255802.

Laske, G., G. Masters, Z. Ma, and M. Pasyanos (2013), Update on CRUST1.0—A 1-degree global model of Earth's crust, In EGU General Assembly Conference Abstracts , vol. 15, p. 2658.

Milne, W. G. (1970), The Snipe Lake, Alberta earthquake of March 8, 1970, *Can. J. Earth Sci.*, *7*, 1564–1567, doi:10.1139/e70-148.

Oprsal, I., and L. Eisner (2014), Cross-correlation—An objective tool to indicate induced seismicity, *Geophys. J. Int.*, *196*(3), 1536–1543.

Parotidis, M., S. A. Shapiro, and E. Rothert (2004), Back front of seismicity induced after termination of borehole fluid injection, *Geophys. Res. Lett.*, *31*, L02612, doi:10.1029/2003GL018987.

Pavlis, G. L., F. Vernon, D. Harvey, and D. Quinlan (2004), The generalized earthquake-location (GENLOC) package: An earthquake-location library, *Comput. Geosci.*, *30*, 1079–1091, doi:10.1016/j.cageo.2004.06.010.

Raleigh, C. B., J. H. Healy, and J. D. Bredehoeft (1976), An experiment in earthquake control at Rangley, Colorado, *Science*, *191*, 1230–1237, doi:10.1126/science.191.4233.1230.

Rebollar, C. J., E. R. Kanasewich, and E. Nyland (1982), Source parameters from shallow events in the Rocky Mountain House earthquake swarm, *Can. J. Earth Sci.*, *19*, 907–918, doi:10.1139/e82-076.

Rebollar, C. J., E. R. Kanasewich, and E. Nyland (1984), Focal depths and source parameters of the Rocky Mountain House earthquake swarm from digital data at Edmonton, *Can. J. Earth Sci.*, *21*, 1105–1113, doi:10.1139/e84-115.

Reiter, K., O. Heidbach, D. Schmitt, K. Haug, M. Ziegler, and I. Moeck (2014), A revised crustal stress orientation database for Canada, *Tectonophysics*, *636*, 111–124, doi:10.1016/j.tecto.2014.08.006.

Reyes, C. G., and M. E. West (2011), The Waveform Suite: A robust platform for manipulating waveforms in MATLAB, *Seismol. Res. Lett.*, *82*, 104–110, doi:10.1785/gssrl.82.1.104.

Schaff, D. P. (2008), Semiempirical statistics of correlation-detector performance, *Bull. Seismol. Soc. Am.*, *98*, 1495–1507, doi:10.1785/0120060263.

Schaff, D. P., and F. Waldhauser (2010), One magnitude unit reduction in detection threshold by cross correlation applied to Parkfield (California) and China seismicity, *Bull. Seismol. Soc. Am.*, *100*, 3224–3238, doi:10.1785/0120100042.

Schultz, R., V. Stern, and Y. J. Gu (2014), An investigation of seismicity clustered near the Cordel Field, west central Alberta, and its relation to a nearby disposal well, *J. Geophys. Res. Solid Earth*, *119*, 3410–3423, doi:10.1002/2013JB010836.

Schultz, R., V. Stern, Y. J. Gu, and D. Eaton (2015), Detection threshold and location resolution of the Alberta Geological Survey earthquake catalogue, *Seismol. Res. Lett.*, *86*(2A), 385–397, doi:10.1785/0220140203.

Shapiro, S. A., and C. Dinske (2009), Fluid-induced seismicity: Pressure diffusion and hydraulic fracturing, *Geophys. Prospect.*, *57*(2), 301–310, doi:10.1111/j.1365-2478.2008.00770.x.

Skoumal, R. J., M. R. Brudzinski, and B. S. Currie (2015), Earthquakes induced by hydraulic fracturing in Poland Township, Ohio, *Bull. Seismol. Soc. Am.*, *105*, 189–197, doi:10.1785/0120140168.

Stern, V. H., R. J. Schultz, L. Shen, Y. J. Gu, and D. W. Eaton (2013), Alberta earthquake catalogue, Version 1.0: September 2006 through December 2010, *Alberta Geol. Surv. Open File Rep., 2013-15,* 36 pp.

Telesca, L. (2010), Analysis of the cross-correlation between seismicity and water level in the Koyna Area of India, *Bull. Seismol. Soc. Am.*, *100*, 2317–2321, doi:10.1785/0120090392.

Waldhauser, F. (2001), HypoDD: A computer program to compute double-difference earthquake locations, *U.S. Geol. Surv. Open File Rep., 01-113*, 25 pp.

Waldhauser, F., and W. L. Ellsworth (2000), A double difference earthquakes location algorithm: Method and application to the northern Hayward Fault, California, *Bull. Seismol. Soc. Am.*, *90*, 1353–1368, doi:10.1785/0120000006.

Wessel, P., and W. H. Smith (1998), New, improved version of Generic Mapping Tools released, *Eos Trans. AGU*, *79*(47), 579–579, doi:10.1029/98EO00426.

Wetmiller, R. J. (1986), Earthquakes near Rocky Mountain House, Alberta, and their relationship to gas production facilities, *Can. J. Earth Sci.*, *23*, 172–181, doi:10.1139/e86-020.

Zhang, Y., et al. (2013), Hydrogeologic controls on induced seismicity in crystalline basement rocks due to fluid injection into basal reservoirs, *Groundwater*, *51*(4), 525–538, doi:10.1111/gwat.12071.